ISSN 1674-1056
http://cpb.iphy.ac.cn
http://iopscience.iop.org/cpb
中国物理 B
Chinese Physics
中国物理
Chinese Physics B

Analysis of optical properties of bio-smoke materials in the 0.25-14 μm band

Xinying Zhao(赵欣颖), Yihua Hu(胡以华), Youlin Gu(顾有林), Xi Chen(陈曦), Xinyu Wang(王新宇), Peng Wang(王鹏), Xiao Dong(董骁)

Citation: Chin. Phys. B . 2019, 28(3): 034201. **doi:** 10.1088/1674-1056/28/3/034201
Journal homepage: http://cpb.iphy.ac.cn; http://iopscience.iop.org/cpb

What follows is a list of articles you may be interested in

Microparticle collection for water purification based on laser-induced convection

Zhi-Hai Liu(刘志海), Jiao-Jie Lei(雷皎洁), Yu Zhang(张羽), Ya-Xun Zhang(张亚勋), Xing-Hua Yang(杨兴华), Jian-Zhong Zhang(张建中), Yun Yang(杨军), Li-Bo Yuan(苑立波)

Chin. Phys. B . 2018, 27(5): 054209. **doi:** 10.1088/1674-1056/27/5/054209

Cavity optomechanics: Manipulating photons and phonons towards the single-photon strong coupling

Yu-long Liu(刘玉龙), Chong Wang(王冲), Jing Zhang(张靖), Yu-xi Liu(刘玉玺)

Chin. Phys. B . 2018, 27(2): 024204. **doi:** 10.1088/1674-1056/27/2/024204

Control of microwave signals using bichromatic electromechanically induced transparency in multimode circuit electromechanical systems

Cheng Jiang(江成), Yuanshun Cui(崔元顺), Xintian Bian(边心田), Xiaowei Li(李晓薇), Guibin Chen(陈贵宾)

Chin. Phys. B . 2016, 25(5): 054204. **doi:** 10.1088/1674-1056/25/5/054204

Stationary entanglement between two nanomechanical oscillators induced by Coulomb interaction

Qin Wu(吴琴), Yin Xiao(肖银), Zhi-Ming Zhang(张智明)

Chin. Phys. B . 2016, 25(1): 014203. **doi:** 10.1088/1674-1056/25/1/014203

Movement of a millimeter-sized oil drop pushed by optical force

Zhang Li, She Wei-Long

Chin. Phys. B . 2015, 24(10): 104207. **doi:** 10.1088/1674-1056/24/10/104207

Analysis of optical properties of bio-smoke materials in the 0.25–14 μm band*

Xinying Zhao(赵欣颖)[1,2], Yihua Hu(胡以华)[1,2,†], Youlin Gu(顾有林)[1,2], Xi Chen(陈曦)[1,2], Xinyu Wang(王新宇)[1,2], Peng Wang(王鹏)[3], and Xiao Dong(董骁)[1,2]

[1] *State Key Laboratory of Pulsed Power Laser Technology, National University of Defense Technology, Hefei* 230037, *China*
[2] *Anhui Province Key Laboratory of Electronic Restriction, National University of Defense Technology, Hefei* 230037, *China*
[3] *Key Laboratory of Ion Beam Bioengineering, Hefei Institutes of Physical Science, Chinese Academy of Sciences, Hefei* 230001, *China*

(Received 14 December 2018; revised manuscript received 9 January 2019; published online 22 February 2019)

At present, research into optical properties of bio-smoke materials mostly concentrates on single band or single germplasm. Herein, we measured the spectral reflectance of three eukaryotic bio-smoke materials and three prokaryotic bio-smoke materials in the waveband from 0.25 μm to 14 μm. Based on the Kramers–Kroning algorithm, the complex refractive index $m(\lambda)$ was calculated and the Fourier-transform infrared (FTIR) spectra of materials were analyzed. The results show that $n(\lambda)$ of bio-smoke materials varies between 1.1–2, and $n(\lambda)$ values in the visible light to near-infrared wavebands are significantly larger than those in other wavebands. The $k(\lambda)$ of bio-smoke materials varies between 0–0.4. At 6–6.5 μm, $k(\lambda)$ of prokaryotic materials is 3 times that of eukaryotic materials, which is caused by C=O stretching vibration of amide I and C–N stretching vibration of amide II in proteins. At 2.5–3 μm and 9.75 μm, $k(\lambda)$ values of eukaryotic bio-smoke materials are nearly 2 times that of prokaryotic ones. The absorption peak at 2.5–3 μm is mainly triggered by C–H stretching vibration in lipid and O–H stretching vibration in bound water. The absorption peak at 9.75 μm is mainly caused by symmetric stretching vibration of PO_2^- in nucleic acids.

Keywords: bio-smoke materials, complex refractive index, eukaryotic, prokaryotic

PACS: 28.41.Qb, 42.50.Wk, 42.70.–a **DOI:** 10.1088/1674-1056/28/3/034201

1. Introduction

A majority of solid and liquid particles suspended in the atmosphere are generated due to biological activities in the terrestrial and aquatic environments. These tiny particles containing microbes or their metabolic products are generally called bioaerosols.[1] The particle number concentration of bioaerosols can account for up to about 30% of that of atmospheric aerosols, and even up to 80% in tropical rainforest regions.[2,3] The main components of microbes in bioaerosols include bacterium, fungus, archaea, and virus.[4] There are eukaryotic and prokaryotic microbes according to the differences in cell structures of microbes. Under natural atmospheric conditions, bacteria (belonging to prokaryotic microbes) and fungus (belonging to eukaryotic microbes) account for 70%–86% and 13%–21% of the total components of bioaerosols, respectively.[5,6] As an important part of the atmosphere, bioaerosols can influence atmospheric radiation characteristics through absorption or scattering. Spankuch *et al.*[7] showed that as the concentration of pine pollen in local areas increases, the atmospheric infrared flux significantly decreases, implying that the emission of certain pollens can result in local climate warming. By using chemical tracers and multiple regression statistical analysis, it can be seen that up to 47% of light absorption above the Amazon rainforest is caused by bio-particles in atmosphere in wet seasons.[8] Even in the transition period from wet season to dry season, the light absorption of bio-particles still accounts for 35% of atmospheric light absorption.[8]

Bioaerosols exhibit excellent electromagnetic shielding properties in the natural environment, and biomaterials are more environmentally friendly and less polluting than conventional smoke materials.[9] Therefore, research into the development of biomaterials into environmentally friendly aerosol materials has drawn the interest of researchers. By using reflectance and transmission spectra, together with Kramers–Kroning (K–K) analysis, Tuminello[10] measured the optical constant *m* of *Bacillus subtilis* in the 0.2–2.5 μm wavelength range, revealing that the values of optical constant *m* of *Bacillus subtilis* in thin film, tablet, aqueous solution, and glycerite are different. Gittins *et al.*[11] measured the infrared extinction spectra of *Bacillus subtilis* atomized in air in a laboratory smog chamber within 2.7–12 μm waveband. The experiment suggested that at 9.65 μm, the peak of extinction coefficient of a single *Bacillus subtilis* spore is obtained through transmission measurement as being about $1.6 \times 10^{-8}/\mathrm{cm}^2$. Gurton[12] detected the infrared extinction spectra of granu-

*Project supported by the National Natural Science Foundation of China (Grant Nos. 61271353 and 60908033) and the Natural Science Foundation of Anhui Province, China (Grant No. 1408085MKL47).

†Corresponding author. E-mail: skl_hyh@163.com

© 2019 Chinese Physical Society and IOP Publishing Ltd

lar *Bacillus* spp. in the 3–13 μm waveband in a laboratory smog chamber and explained the transmission data during the experiment by calculating the complex refractive index *m* of the granular *Bacillus* spp. based on Mie scattering theory. According to transmission and reflectance spectra, Wang *et al.*[13] calculated the optical constants of seven microbial particles in the 2.5–25 μm wavelength range and measured the electromagnetic attenuation properties of microbial particles through smog chamber experiments. Professor Hu's research team[14–18] studied the extinction mechanism of bioaerosols and explored the potential of bioaerosol as a new smoke material through smoke box experiments.

In order to better develop bioaerosol into bio-smoke material, we need to further study the following two aspects. For one thing, previously, scholars mainly explored the optical properties of specific single microbes, which is conducive to understanding special cases concerning the optical properties of microbes. However, the universality and particularity of the optical properties of bioaerosols cannot be concluded therefrom. For another, previous studies were merely concerned with a single optical band, concentrating on the infrared. The studies into broad-band optical properties of microbes in ultraviolet (UV), visible light, and infrared waves were rarely involved, which is not conducive to the analysis of the influences of bioaerosols on atmospheric radiation characteristics. To address these drawbacks, we are supposed to cover in our research a wider range of species of microbes and wave bands. We selected 6 potential bio-smoke materials for research: EM01 spore, EM02 spore, EM03 spore, PM01 bacillus, PM02 bacillus, and PM03 bacillus. According to the cellular structure, the six microbes are divided into eukaryotic (spores) and prokaryotic (bacilli) microbes. In the study, the general characteristics of optical properties of bio-smoke materials in the 0.25–14 μm wavelength range are assessed to allow the analysis of differences in optical properties of eukaryotic and prokaryotic materials at 0.25–14 μm. The results of the study help us to obtain the broadband optical properties of bio-smoke materials and provide a theoretical basis for the development of new functional materials.

2. Materials and methods

Spores and bacilli are provided by the Key Laboratory of Ion Beam Bioengineering, Chinese Academy of Sciences. They were isolated by the laboratory and stored at −80 ℃ in sterilized cryovials containing 10% glycerol (in 0.02% Tween-80 solution). We have optimized fermentation conditions and improved collection efficiency for the biomaterials production.[19,20] The operating steps are as follows: bacterial species activation → shake flask culture → large-scale tank fermentation → centrifugation → pure water cleaning → drying in vacuum freeze dryer → ultra-fine crushing in Chinese medicine crusher (see Supplementary Material Section 1 for specific steps). And then the biomaterials are stored in dessicators containing silica gel absorbent (Fig. S1 in Supplementary Material) and sealed and bagged at room temperature (Fig. S2 in Supplementary Material). In order to make the bio-smoke materials environmentally friendly, pollution-free, and floating in the air, we have inactivated and pulverized the material. The microscopic structural morphologies of the bio-smoke materials were observed by using a scanning electron microscope (SEM) (Sirion 200, FEI Ltd., Hillsboro, Oregon, USA), as shown in Fig. 1. It can be seen that PM01, PM02, and PM03 spores are spherical in shape with a radius of 1–2 μm, and the original morphology remains well after inactivation, drying, and pulverization. However, the original form of the other three bacilli materials cannot be easily recognized after crushing, with agglomeration.[21]

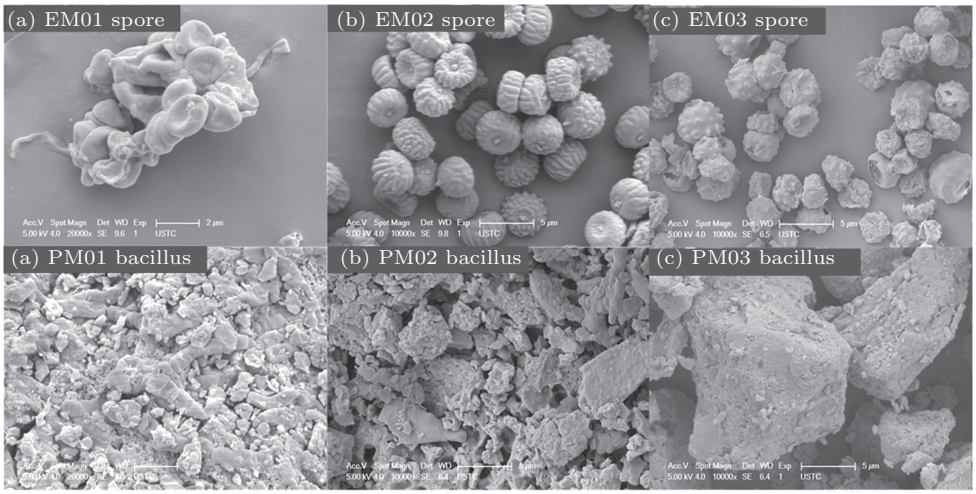


Fig. 1. SEM images of six prepared bio-smoke materials. (a) EM01 spores (20000× magnification, scale: 2 μm), (b) EM02 spores (10000× magnification, scale: 5 μm), (c) EM03 spores (10000× magnification, scale: 5 μm), (d) PM01 (20000× magnification, scale: 2 μm), (e) PM02 (10000× magnification, scale: 5 μm), and (f) PM03 (10000× magnification, scale: 5 μm).

The complex refractive index m of bio-smoke materials in the 0.25–14 μm waveband can be calculated by using the spectral reflectance of materials and the Kramers–Kroning algorithm,[22–25] as mentioned in our previous work.[17,18,26] The spectral reflectance of bio-smoke material tablets in the waveband from 0.25 μm to 2.5 μm was measured by applying the U-4100 spectrophotometer (Hitachi U-4100, Hitachi Ltd., Tokyo, Japan) for UV, visible (Vis) light, and near infrared (NIR). And the spectral reflectance in 2.5 μm to 14 μm was measured by a Fourier infrared spectrometer (MAGNA-IR 750, Nicolet Instrument Co., USA) with a matched microscope (Continuμm, Nicolet Instrument Co., USA), as shown in Figs. 2(a) and 2(c). The specific steps for measuring the reflectivity of biomaterial tablets are in Supplementary Material Section 2.

Based on the measured reflection spectrum, m of bio-smoke materials in the 0.25–14 μm wavelength range was calculated using the K–K relationship. The reflective phase shift $\Theta(\lambda)$ can be expressed as[26]

$$\Theta(\lambda) = \frac{\lambda}{\pi} P \int_0^{\infty} \frac{\ln R(\lambda')}{(\lambda'^2 - \lambda^2)} \mathrm{d}\lambda', \tag{1}$$

where $R(\lambda)$ is the vertical reflectivity, λ' is an integral variable whose range of variation is $(0, +\infty)$ and $\lambda' \neq \lambda$, P is the Cauchy principal value function, and λ is the wavelength. $m(\lambda) = n(\lambda) + k(\lambda)\mathrm{i}$, where $n(\lambda)$ and $k(\lambda)$ are given by[26]

$$n(\lambda) = \frac{R(\lambda)}{1 + R(\lambda) + 2\sqrt{R(\lambda)}\cos\Theta(\lambda)}, \tag{2}$$

$$k(\lambda) = \frac{2\sqrt{R(\lambda)}\cos\Theta(\lambda)}{1 + R(\lambda) + 2\sqrt{R(\lambda)}\cos\Theta(\lambda)}. \tag{3}$$

From Eq. (1), $R(\lambda)$ should be obtained over the full bandwidth to calculate $m(\lambda)$. However, in actual experimental measurements, $R(\lambda)$ can be measured only within the limited bandwidth (0.25–14 μm). The constant extrapolation method was used to expand the range of reflectivities. A value of 100 μm was used as the upper limit of the integral because the reflectivity above 100 μm had little effect on $m(\lambda)$ in the 0.25–14 μm wavelength range. R(0–0.25 μm) = R(0.25 μm), and R(14–100 μm) = R(14 μm). Therefore, $R(\lambda)$ over the entire integral range (0–100 μm) was acquired.

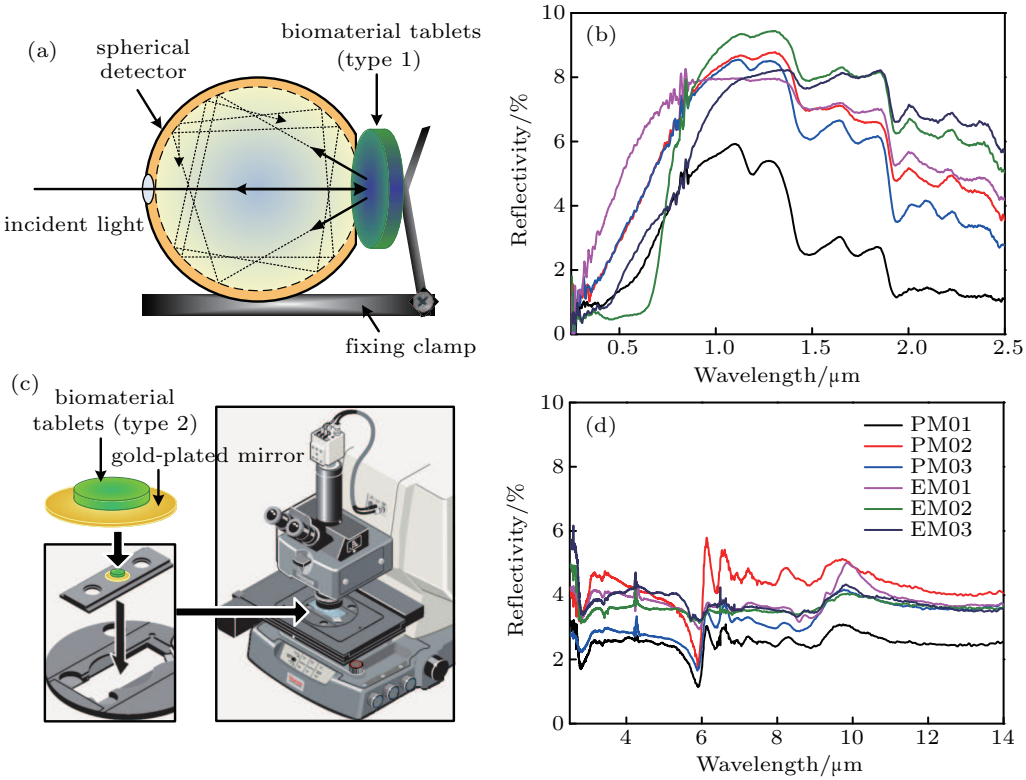


Fig. 2. Spectral reflectance measurement of bio-smoke materials in the 0.25 μm to 14 μm band. (a) Operational principle of the measurement of the reflection spectrum using a spectrophotometer. (b) Reflectivity of bio-smoke materials in 0.25–2.5 μm. (c) Schematic diagram of installation of bio-smoke material tablets and a gold-plated mirror on the microscope stage. (d) Reflectivity of bio-smoke materials in 2.5–14 μm. (b) and (d) share the same legend.

3. Results and discussion

The selected bio-smoke materials can be divided into two groups: eukaryotic and prokaryotic microbes. EM01 spore, EM02 spore, and EM03 spore are eukaryotic microbes while PM01 bacillus, PM02 bacillus, and PM03 bacillus are prokaryotic microbes. According to the data on spectral reflectance of the six materials in the 0.25–14 μm wavelength range, the $m(\lambda)$ values of eukaryotic and prokaryotic bio-smoke materials in the 0.25–14 μm range were calculated by using the K–K algorithm, as shown in Fig. 3.

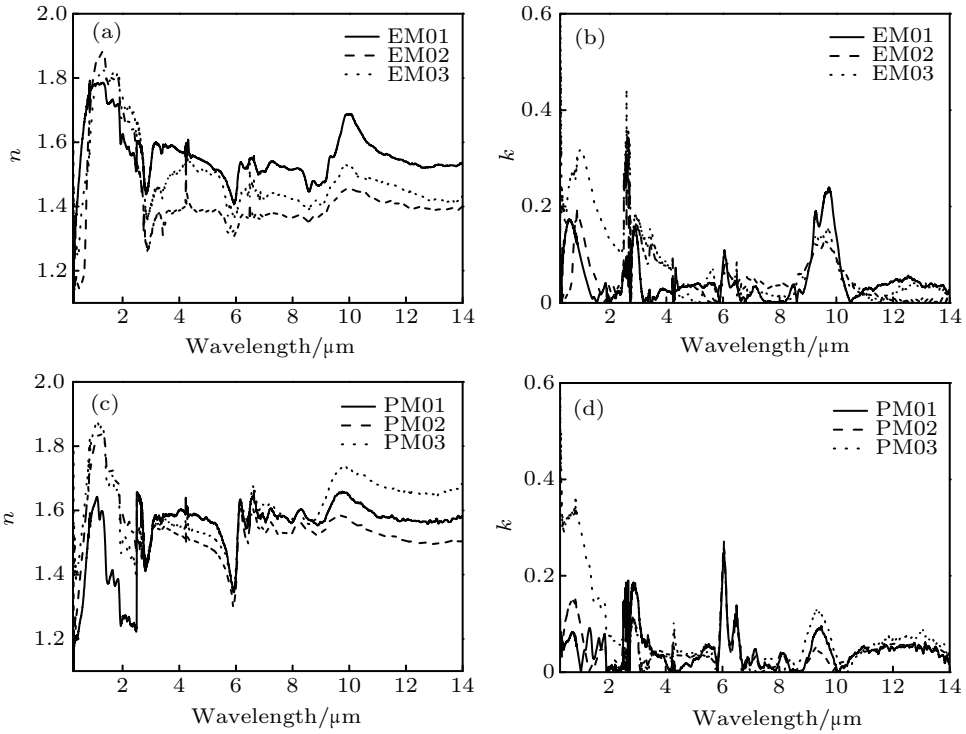


Fig. 3. The $m(\lambda)$ of eukaryotic and prokaryotic bio-smoke materials in the 0.25–14 μm range. (a) $n(\lambda)$ of eukaryotic bio-smoke materials, (b) $k(\lambda)$ of eukaryotic bio-smoke materials, (c) $n(\lambda)$ of prokaryotic bio-smoke materials, and (d) $k(\lambda)$ of prokaryotic bio-smoke materials.

The $n(\lambda)$ depends on the propagation velocity of optical waves in the absorbing medium and is closely related to the wavelength and attributes of the absorbing medium. As shown in Figs. 3(a) and 3(c), $n(\lambda)$ of eukaryotic and prokaryotic bio-smoke materials varies between 1.10–2. The $n(\lambda)$ values in the visible light and near-infrared wavebands are significantly larger than those within the other wavelength ranges. Within the 2.5–14 μm band, $n(\lambda)$ values of prokaryotic bio-smoke materials are larger than that of eukaryotic ones. The $k(\lambda)$ of absorbing media refers to the absorption coefficient, which is determined by the attenuation velocity of optical waves propagating in an absorbing medium. As shown in Figs. 3(b) and 3(d), $k(\lambda)$ of eukaryotic and prokaryotic bio-smoke materials varies between 0–0.4. What should be noted is that $k(\lambda)$ values of eukaryotic materials in the 6–6.5 μm band are less than 0.1 and have no significant peaks compared with $k(\lambda)$ in other wavelength bands. The peak $k(\lambda)$ for prokaryotic materials is found in the 6–6.5 μm band, to be around 0.3, which is 3 times that of eukaryotic materials. At 2.5–3 μm and 9.75 μm, $k(\lambda)$ of eukaryotic bio-smoke materials is nearly 2 times that of prokaryotic ones.

The similarities and differences in $n(\lambda)$ and $k(\lambda)$ of eukaryotic and prokaryotic bio-smoke materials are both closely related to their structures and components. The eukaryocytes include a shaped nucleus (1–3 μm) and multiple organelles (such as mitochondria (about 1 μm) and ribosome (<1 μm)), which perform mitosis. A prokaryotic cell with a simple structure has a particle size in the range of 1–10 μm, and is composed of a cell wall, cytomembrane, cytoplasm, and nuclear zone. The nuclear zone is just a grouping nuclear matter without an interface membrane at the outer side, which is not a shaped nucleus. However, there is circular DNA in the nuclear zone, which makes up the transcription and translation system for genetic information with RNA, enzymes, etc. The main difference in the two types of cells is that prokaryotic cells contain no shaped nucleus, but nucleoid and organelles including only a ribosome. The division method of prokaryotic cells is amitosis. Most prokaryotic cells have cell walls. Organisms in bacterium and archaea kingdoms consist of prokaryotic cells, while protist, fungus, plants, and animals are all made of eukaryocytes. In terms of material composition, all varieties of cells basically contain water, protein, lipid, nucleic acid, etc.[27]

Generally, water in such cells accounts for 85%–90% of cell fresh weight. The water content of adipocytes is relatively low, accounting for 10%–30%.[28] In the present experiment, the bio-smoke materials lose their liquid-state free water after vacuum freeze-drying, while the remaining water is combined with intracellular macromolecules in the form of bound water. Loss of free water will reduce the cytoplasmic density. But as can be seen from Fig. 1, the eukaryotic spore material we prepared has a good morphology after dehydration, with no obvious rupture or obvious voids in the spores. However, the morphology of the prokaryotic material changes after dehydration and pulverization, and there is agglomeration. Due to the different densities of the two materials, $n(\lambda)$ of the eukaryotic materials is generally smaller than that of the prokaryotic materials.

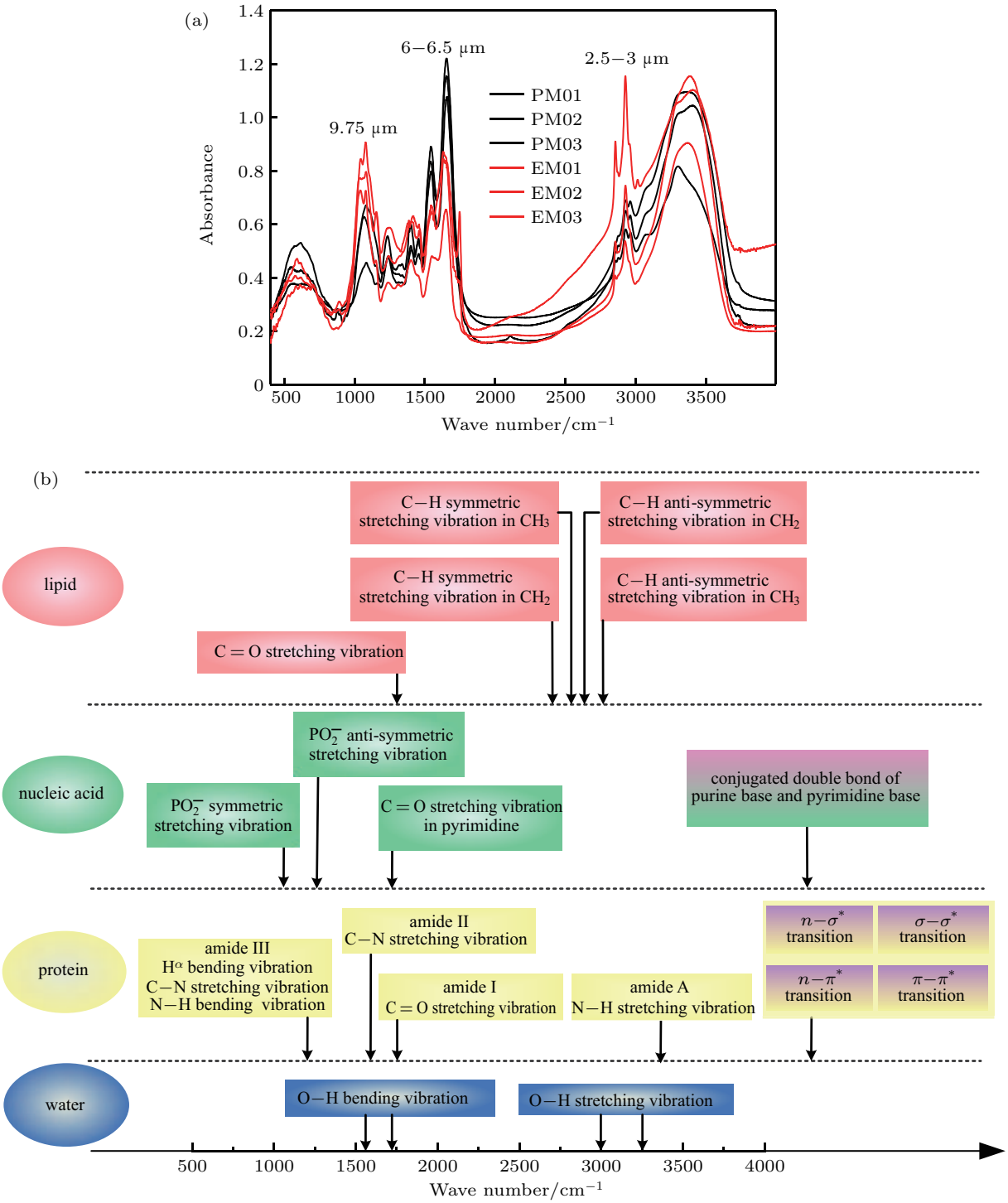


Fig. 4. Schematic diagram of the absorption characteristics of eukaryotic and prokaryotic bio-smoke materials. (a) Absorbance of six bio-smoke materials in the infrared band (400–4000 cm^{-1}). (b) Analysis of infrared absorption peaks of various components of the bio-smoke materials. The absorption peaks of proteins and nucleic acids in the ultraviolet bands (purple parts) in the figure are derived from the literature.[29]

The differences in absorption characteristics of eukaryotic and prokaryotic materials can be analyzed by using infrared spectra of bio-smoke materials. The bio-smoke materials and KBr reagent were ground and mixed in a 1:150 mass ratio to make a tablet, and then the absorbance spectrum of the tablet was measured using the Fourier transform infrared spectrometer (MAGNA-IR 750, Nicolet Instrument Co., USA). The absorbance spectra are shown in Fig. 4(a). As shown in the figure, bio-smoke materials exhibit similar absorption peaks in the 400–4000 cm^{-1} waveband, as determined by absorption characteristics of the compositions of microbial cells, as shown in Fig. 4(b). The basic composition materials of cells include water, protein, lipid, and nucleic acid.[27] Water molecules show significant infrared absorption at 3000–3750 cm^{-1} (anti-symmetric and symmetric stretching vibration of H_2O) and 1600–1700 cm^{-1} (bending vibration of H_2O).[30] The main characteristic absorption of protein on Fourier-transform infrared (FTIR) spectra appears

as amide band: amide I at 1600–1700 cm^{-1} (C=O stretching vibration), amide II at 1500–1600 cm^{-1} (C–N stretching vibration), amide III at 1200–1300 cm^{-1} (the vibration is complex, including bending vibration of H^{α}, C–N stretching vibration, and N–H in-plane bending vibration), and amide A around 3300 cm^{-1} (mainly involving N–H stretching vibration). The main characteristic absorption peaks of lipid appear at 2959 cm^{-1} (C–H anti-symmetric stretching vibration in CH_3), 2922 cm^{-1} (C–H anti-symmetric stretching vibration in CH_2), 2872 cm^{-1} (C–H symmetric stretching vibration in CH_3), 2852 cm^{-1} (C–H symmetric stretching vibration in CH_2), and 1741 cm^{-1} (C=O stretching vibration). The characteristic absorption peaks of nucleic acid appear at 1715 cm^{-1} (C=O stretching vibration in pyrimidine), 1220–1250 cm^{-1} (anti-symmetric stretching vibration of PO_2^-), and 1085 cm^{-1} (symmetric stretching vibration of PO_2^-).

In the UV wavelength range, protein and nucleic acid also show strong absorption peaks, as shown in purple in Fig. 4(b). For protein, within the UV wavelength range, the group made of a single bond only involves the σ-bond electron, thus only showing a $\sigma-\sigma^*$ transition. The transition energy of σ-bond electrons is high, thus is difficult to activate. The absorption spectra of groups made of a single bond within the UV wavelength range are located in the far-UV region ($\lambda < 150$ nm). Therefore, the groups in protein molecules (including $-CH_2^-$, C–N, $-CH_3$, and hydrogen bonds) consisting of a single bond exhibit absorption characteristics only in the far-UV region. If the groups made of single bond include various atoms (such as O, N, and S), the groups also contain unshared p-electron pairs apart from σ-bond electrons. Therefore, n$-\sigma^*$ transition can be detected and the absorption peak approximates to, or is in, the near-UV region (200–380 nm). As a consequence, the groups (including $-NH_2$, $-OH$, C–N, and C–S) in protein molecules show absorption peaks at around 200 nm. Apart from σ-bond electrons, π-bond electrons are also found in the unsaturated chemical bonds (such as >C=C<, >C=O, and >C=N−) in protein molecules, which can trigger $\pi-\pi^*$ transition. In this context, the absorption peak appears at around 200 nm in the UV region. When the n-electrons co-exist with a π-bond in protein molecules, n$-\pi^*$ transition occurs to absorb UV waves within the 200–380 nm wavelength range. Purine base and pyrimidine base exhibit conjugated double bonds, which causes the basic group, nucleoside, nucleotide, and nucleic acid to return strong absorption peaks in the UV wavelength range of 240–290 nm.[29]

In Fig. 4(a), the absorbance of eukaryotic materials at 9.75 μm and 2.5–3 μm is significantly higher than that of prokaryotic materials. As shown in Fig. 4(b), the absorption peak at 9.75 μm is mainly caused by symmetric stretching vibration of PO_2^- in nucleic acid in cells while that at 2.5–3 μm is mainly triggered by C–H stretching vibration in lipid in cells and O–H stretching vibration in bound water. The cells of eukaryotic microbes contain a shaped cell nucleus, and a chromosome mainly composed of thread-like DNA and protein; mitochondria and chloroplasts also contain genetic material. For cells of prokaryotic microbes, only nucleoid and plasmid contain genetic materials. By contrast, the amount of genetic material in eukaryocytes is greater than that in prokaryotic cells, which is shown from the perspective of optical characteristics such that the absorption peak of eukaryocytes caused by symmetric stretching vibration of PO_2^- in nucleic acid at 9.75 μm is much greater than that of prokaryotic microbes. Additionally, compared with prokaryotic microbes, eukaryotic microbes not only contain a cytomembrane but also have rich organelle membranes, making up a biological membrane system. The chemical compositions of biological membranes mainly include lipid, protein, and small amounts of saccharides, which separately account for about 50%, 42%, and 2%–8% by mass. Therefore, the absorption peak of eukaryotic microbes caused by C–H stretching vibration in lipid at 2.5–3 μm is significantly higher than that of prokaryotic microbes. The infrared absorption peak of cells at 6–6.5 μm is mainly related to O–H bending vibration in water, C=O stretching vibration of amide I, C–N stretching vibration of amide II in protein molecules, C=O stretching vibration in nucleic acid, and C=O stretching vibration in lipid. Owing to the contents of nucleic acid and lipid in prokaryotic microbes all being lower than those in eukaryotic microbes, and the content of bound water being low after microbial materials were freeze-dried, the strong absorption peak of prokaryotic microbes at 6–6.5 μm is caused by C=O stretching vibration of amide I and C–N stretching vibration of amide II in protein molecules.

4. Conclusions

In this work, Fourier infrared spectrometer was used to measure the reflectivity of materials in the 2.5 μm to 14 μm band. Meanwhile, UV/Vis/NIR spectrophotometer was used to measure the reflectivity of materials in the 0.25 μm to 2.5 μm band, which effectively expands the spectral measurement band of bio-smoke materials. By calculating and comparing the complex refractive index spectra of eukaryotic and prokaryotic bio-smoke materials in the 0.25–14 μm band, we naturally draw the following conclusions: $n(\lambda)$ of eukaryotic and prokaryotic bio-smoke materials varies between 1.1–2, showing the same change trend and location of extreme points. In the visible light to near-infrared wavebands, $n(\lambda)$ values are significantly larger than those of other wavebands. Within the 2.5–14 μm band, $n(\lambda)$ values of prokaryotic bio-smoke materials are larger than that of eukaryotic ones. The $k(\lambda)$ of eukaryotic and prokaryotic bio-smoke materials varies between 0–0.4. The $k(\lambda)$ of prokaryotic materials at 6–6.5 μm is 3 times that of eukaryotic materials. This is caused by C=O

stretching vibration of amide I and C–N stretching vibration of amide II in protein molecules of prokaryotic cells. At 2.5–3 μm and 9.75 μm, $k(\lambda)$ values of eukaryotic bio-smoke materials are nearly 2 times that of prokaryotic ones. The absorption peak at 2.5–3 μm is mainly triggered by C–H stretching vibration in lipid and O–H stretching vibration in bound water. The absorption peak at 9.75 μm is mainly caused by symmetric stretching vibration of PO_2^- in nucleic acid in cells.

Compared with traditional smoke materials, biomaterials have abundant sources, low production costs, less environmental pollution, and great application potential. Since eukaryotic and prokaryotic biomaterials exhibit different extinction capacities at specific wavelengths, we can make bio-smoke materials cover specific light bands. And we can also detect bio-aerosol pollutants by remote sensing and identify pollutant types by analyzing their optical characteristics. The broadband extinction characteristics of bio-smoke materials in the ultraviolet to infrared bands provide a new idea for the development of functional materials.

References

[1] Ariya P A and Amyot M 2004 *Atmos. Environ* **38** 1231
[2] Janine F N, Christopher J K and Bettina W 2016 *Atmos. Res.* **182** 346
[3] Huffman J A 2012 *Atmos. Chem. Phys.* **12** 11997
[4] Pöhlker C, Huffman J A and Pöschl U 2012 *Atmos. Meas. Tech.* **5** 37
[5] Bowers R, Clements N, Emerson J B, Wiedinmyer C, Hannigan M P and Fierer N 2013 *Environ. Sci. Technol.* **47** 12097
[6] Cao C, Jiang W, Wang B, Fang J, Lang J, Tian G, Jiang J and Zhu T F 2014 *Environ. Sci. Technol.* **48** 1499
[7] Spänkuch D, Döhler W and Güldner J 2000 *J. Geophys. Res.* **105** 17341
[8] Guyon P 2004 *Atmos. Environ* **38** 1039
[9] Shu X M, Fang J, Shao Q, Yuan H Y and Fan W C 2006 *Chin. Phys. Lett.* **23** 385
[10] Tuminello P S, Arakawa E T, Khare B N, Wrobel J M, Querry M R and Milham M E 1997 *Appl. Opt.* **36** 2818
[11] Gittins C, Piper L, Rawlins W and Marinelli W 1999 *Field Anal. Chem. Technol.* **3** 274
[12] Gurton K P, Ligon D and Kvavilashvili R 2001 *Appl. Optics* **40** 4443
[13] Wang P, Liu H X and Zhao Y Z 2016 *Appl. Spectrosc.* **70** 1456
[14] Zhao X Y, Hu Y H and Gu Y L 2015 *Acta Opt. Sin.* **35** 0616001 (in Chinese)
[15] Sun D J, Hu Y H, Gu Y L and Wang Y 2013 *Acta Phys. Sin.* **62** 094218 (in Chinese)
[16] Li L, Hu Y H, Chen W, Zhao Y Z and Chen S J 2015 *Spectrosc. Spect. Anal.* **35** 89 (in Chinese)
[17] Gu Y L, Hu Y H, Zhao X Y, Chen X and Wang P 2018 *Opt. Express* **26** 15842
[18] Gu Y L, Hu Y H, Zhao X Y, Chen X, Wang P and Zheng Z M 2019 *Optik* **176** 535
[19] Liu H X and Zhao X S 2015 *BMC Microbiol.* **15** 267
[20] Liu H X, Wang P, Hu Y H and Zhao G H 2015 *Biocontrol Sci. Technol.* **25** 1011
[21] Pang H C, Luo S Z, Long X G and An Z 2006 *Chin. Phys. Lett.* **23** 3238
[22] Segal-Rosenheimer M and Linker R 2009 *J. Quant. Spectrosc. Radiat. Transfer* **110** 1147
[23] Lai J C, Li Z H and He A Z 2005 *Chin. Phys. Lett.* **22** 332
[24] Sun W F, Wang X K and Zhang Y 2009 *Chin. Phys. Lett.* **26** 114210
[25] Ji Y Q, Jiang Y G, Liu H S, Wang L S and Liu D D 2014 *Chin. Phys. Lett.* **31** 46401
[26] Li L, Hu Y H, Gu Y L and Zhao X Y 2017 *Appl. Spectrosc.* **71** 2555
[27] Miller L M and Dumas P 2010 *Curr. Opin. Struct. Biol.* **20** 649
[28] Ren L and Li J 1965 *Food Sci.* **30** 388
[29] Pace N R 1997 *Science* **276** 734
[30] Quaroni L and Zlateva T 2011 *Analyst* **136** 3219